



Measurements of Particle Fluxes, Electric Fields, and Lightning Occurrences at the Aragats Space-Environmental Center (ASEC)

A. CHILINGARIAN,¹ T. KARAPETYAN,¹ B. SARGSYAN,¹ Y. KHANIKYANC,¹ and S. CHILINGARYAN^{1,2}

Abstract—To catalyze transformative advancements in High-energy Physics in the Atmosphere (HEPA), a comprehensive understanding of particle fluxes, electric fields, and lightning occurrences across atmospheric layers is imperative. This paper elucidates the instrumentation and capabilities of the Aragats Space-Environmental Center (ASEC), which encompasses measurement tools for various cosmic ray species, near-surface electric fields, and lightning events integrated across high-mountain research station at slopes of Mt. Aragats and the highest mountains of Eastern Europe and Germany. Through these measurements, we aim to elucidate models of particle acceleration mechanisms and the charge distribution within the lower atmosphere. We introduce an Advanced Data Extraction Infrastructure (ADEI) integrated with sophisticated statistical analysis tools to facilitate rapid access to this wealth of data. Despite the significance of these atmospheric processes, the intricate interplay between thundercloud electrification, lightning activity, wideband radio emissions, and particle fluxes remains poorly understood. A particularly compelling avenue of inquiry lies in exploring the relationship between high-energy atmospheric phenomena, intracloud electric fields, and lightning initiation. Furthermore, investigations into accelerated structures within geospace plasmas hold promise for shedding light on particle acceleration processes, potentially extending to higher energies within analogous structures in cosmic plasmas. This paper also examines practical methodologies for extracting meaningful physical insights from temporal datasets, such as correlating surges in particle flux intensity with variations in near-surface electric field strength and precipitation patterns. Additionally, we explore the utility of wideband field and interferometer antenna signals in this context, offering valuable avenues for further research and analysis. Through these endeavors, we aim to deepen our understanding of high-energy atmospheric processes and their broader implications for terrestrial and cosmic phenomena.

Keywords: Atmospheric electric fields, electron acceleration, lightning location, particle detectors.

1. Introduction

One of the recognized leaders in contemporary investigations of geophysical phenomena using multidetector monitoring of the atmospheric phenomena is Cosmic Ray Division (CRD) of the A. Alikhanyan National Scientific Laboratory of Armenia and its Aragats Space Environmental Center (ASEC, Chilingarian et al., 2003, 2005). At CRD's Aragats and Nor Amberd research stations, the networks of detectors registering near-surface electric field (NSEF), atmospheric parameters, lightning flashes, and fluxes of various species of cosmic rays (CR) operate 24/7, providing important information on various high-energy physics and atmospheric processes.

Four peaks of Aragats: northern (highest, 4090 m), western (3995 m), southern (3888 m), and eastern (3908 m), form the edges of a volcanic crater that exploded 1.5 million years ago and covered half of Armenia with tuff and basalt rocks. The Aragats research station is located on a flat elevation of volcanic origin at an altitude of 3200 m near the large lake of glacial origin Kari (latitude: 40.4713N, longitude: 44.1819E). The daily outside temperature from 2011 (start of continuous measurements) to 2024, varies within (− 25 to + 20C) and near-surface electric field within (− 30 to + 30) kV/m, although the peak values corresponding to the lightning flashes can be larger. Snow covers the ground for 120 days a year with an average thickness of over a meter.

Since 1943, cosmic ray research on Aragats hasn't stopped during the most difficult years in the history of modern Armenia. The early history of research on Argats is described in Chilingarian et. al. (2009). At

¹ Alikhanyan National Laboratory (Yerevan Physics Institute), 0036 Yerevan, Armenia. E-mail: chili@aragats.am; ktigran79@gmail.com; balabeksargsyan@gmail.com; khanikyanc@yerphi.am; csa@suren.me

² Karlsruhe Institute of Technology, Hermann-Von-Helmholtz-Platz, 176344 Eggenstein-Leopoldshafen, Germany.

the end of the last century, we finished experiments with large ground-based installations registering particle fluxes from the interactions of protons and nuclei (extensive air showers EASs), accelerated to ultrahigh energies by galactic and extragalactic accelerators. We first obtain the energy spectra of light and heavy nuclei separately by the MAKET-ANI surface array (Chilingarian et al., 2004, 2007); the raw data is available from the (KCDC, 2024). In the old days, the physics of the atmosphere did not seem attractive to us; however, starting to study atmospheric electricity and its modulation effects, we realized that using networks of detectors, along with electric field sensors, lightning locators, automatic weather stations and panoramic cameras, we can reach new quality research and create a new scientific direction, which is now called high-energy physics in the atmosphere (HEPA, Dwyer et al., 2012). The location of our station on the plateau under the southern summit of Mount Aragats near the large mountain lake Kare-lich facilitated the observation of numerous events of thunderstorm ground enhancements (TGEs, Chilingarian et al., 2010, 2011, 2020b), abrupt, impulsive enhancement of the count rates of electrons, gamma rays, and rarely neutrons measured by particle detectors located on the Earth's surface under thunderclouds. Aragats is ideal for the TGE research, especially in Spring and Autumn when thunderstorm clouds descend directly to the station.

Central to HEPA is the phenomenon of free electron acceleration within atmospheric electric fields (AEF). Electrons generated in extensive air showers (EASs, Auger et al., 1939) can undergo substantial energy gains within these fields, initiating electron-gamma ray avalanches. This process, known as Relativistic Runaway Electron Avalanches (RREAs, Alexeenko et al., 2002; Babich, et al., 2001; Dwyer, 2007; Gurevich et al., 1992), persists if the electric field maintains specific conditions within the large-scale AEF. The RREA mechanism efficiently multiplies and accelerates electrons initiated avalanches afterward detected on Earth's surface as TGEs, in space as Terrestrial Gamma-ray Flashes (TGFs, Fishman et al., 1994), or in the upper atmosphere as gamma glows (Kelley et al., 2015). The initiation of RREAs is contingent upon factors such as electric field strength, spatial extent, and air

density (Dwyer, 2003). However, the phenomena of TGFs, TGEs, and gamma glows can be analyzed within the same RREA framework. Differences in their observational characteristics could be explained not by distinct mechanisms of their origination but by divergences in experimental arrangements (Chilingarian, 2024). ALOFT data (Ostgaard et al., 2023) reveals that RREAs registered in the upper atmosphere resemble the RREAs developed in the lower atmosphere, including their durations, highlighting how proximity to the source influences our interpretation of these events.

Observationally, if RREAs terminate at heights exceeding 100 m from the ground, TGEs contain mostly gamma rays; electrons will fast absorbed after leaving the electric field. However, for 4 of 5 largest TGEs (flux enhancement > 100%, Chilingarian et al., 2024a) registered on Aragats in 2023, the electric field heights above the ground were less than 100 m, and the electron energy spectrum with energies up to 50 MeV was successfully recovered. The unique peculiarity of spectrometers operated on Aragats is the possibility to separate charged and neutral fluxes and a much wider particle energy range (up to 100 MeV) compared with standard gamma spectrometers (usually 3–10 MeV).

Noteworthy are wintertime gamma glows, akin to TGEs containing only gamma rays due to the larger height of the electric field above the ground, commonly observed along the northwest coast of Japan. These occurrences result from the convergence of cold and dry Siberian winds with the warm Tsushima current, inducing upward air currents that precipitate thunderstorm formation (Torii et al., 2011). The Airborne detectors have also captured these gamma-ray glows, which stem from electron acceleration within the space bounded by the positive cloud top layer and the negative screening layer above it (Ostgaard et al. 2019).

Enhancing our understanding of TGEs is complemented by continuously monitoring environmental parameters through weather stations, electric field sensors, and all-sky cameras. The correlation analyses of the multivariate measurements led to the development of models elucidating the interactions of electrons, positrons, muons, neutrons, and photons with the atmosphere and electric fields therein

(Chilingarian et al., 2022a, 2022b, 2022c). Pioneering work led by physicists from the Yerevan Physics Institute, in collaboration with colleagues from the SEVAN network, initiated the first-ever TGE search campaign employing SEVAN detectors at the highest peaks in Eastern Europe and Germany (Chilingarian et al., 2024b). This exhaustive campaign, spanning a decade and operating round-the-clock, yielded numerous TGE detections at prominent mountain sites, including Aragats, Lomnicky Stit, Musala, and Zugspitze (Chilingarian et al., 2024b). Joint analysis of these observations unveiled that despite the diverse characteristics of detected TGEs in intensity, they exhibit significant commonalities. Notably, the most prominent TGEs typically endure for mere minutes, during which particle fluxes surge to tens or even hundreds of times their fair-weather values. Intriguingly, TGEs often experience abrupt terminations coinciding with lightning flashes (Chilingarian et al., 2015), albeit lightning activity appears to be suppressed during TGE events (Chilingarian et al., 2017b). Recent publications have cataloged 650 TGE events observed on Aragats (Chilingarian et al., 2022c) and 80 gamma-ray glows detected along the western seashore of Japan (Wada et al., 2021), providing compelling evidence that the RREA mechanism operates universally in thunderous atmospheres worldwide.

Time series of count rates of particle fluxes, magnetic and electric fields, meteorological conditions, and lightning occurrences from research stations located on slopes of Mt. Aragats and in Yerevan continuously enter databases at CRD headquarters in Yerevan. The nodes of the SEVAN network in Eastern Europe also send data on particle fluxes and electric fields to databases for joint analyses. The stream of “big” data from all detectors is analyzed with the Advanced Data Extraction Infrastructure (ADEI, Chilingaryan et al., 2010) developed in collaboration with the Karlsruhe Institute of Technology (KIT). A user-friendly interface interactively visualizes the multiple time series and selects relevant parameters for different research objectives. ADEI provides analysis tools and services to utilize the scientific potential of multivariate correlation analysis. We try to fully utilize the concept of “big”

data when an enormous amount of observations leads to “new” physics unprecedentedly fast and precise.

This paper presents the results of joint analyses of particle fluxes, electric fields, and lightning occurrences. We will also demonstrate how the ADEI deals with multivariate measurements with tools for multivariate visualization and correlation.

2. The Equipment Used for Electric Field Measurements on the Slopes of Mt. Aragats and in Yerevan City

Below are briefly described the instruments used at the ASEC to measure AEF, lightning location, and radio emission from the atmospheric discharges. Afterward, we will discuss several examples of data analysis tasks using measurements of particle fluxes and corresponding atmospheric electricity disturbances.

The near-surface electric field (NSEF) is continuously monitored by a network of commercially available field mills (Model EFM-100, BOLTEK1, 2024), three of which are placed at the Aragats station, one at the Nor Amberd station at a distance of 12.8 km from Aragats, one in Burakan village, 15 km from Aragats, and one at the Yerevan station, at a distance of 39.1 km from Aragats (Fig. 1). The distances between the three field mills at Aragats are 80 m, 270 m, and 290 m. The sensitivity distance of EFM-100 for the lightning location estimation is 33 km, and the response time of the instrument is 100 ms. The electrostatic field changes are recorded at a sampling interval of 50 ms. Data on the continuous monitoring of the NSEF starting from 2010 (1 s time series) are available via ADEI.

The lightning activity from 30 to 480 km is monitored by Boltek’s Storm Tracker (lightning detection system, BOLTEK2, 2024). Storm tracker defines four types of lightning types (CG−, CG+, cloud-to-ground negative and positive, IC−, IC+ intracloud positive and negative) in radii up to 480 km around the location of its antenna. By examining the time-slices of the lightning activity, we determine from which direction the storm is coming, and, finally, by putting on the map all lightning



Figure 1

The map shows the location of EFM-100 electric field mills on the slopes of Mt. Aragats and in Yerevan

occurrences, we can see if the storm's active zone goes above the stations or misses them, see Fig. 2.

Meteorological conditions are measured by Vantage Pro2 Plus automatic weather stations from Davis Instruments. The weather station includes a rain collector, temperature and humidity sensors, an anemometer, a solar radiation sensor, and a UV sensor. Weather stations are in Aragats (2 units), Nor Amberd, Burakan, and Yerevan. One-minute time series are available from 2010.

The ALL SKY CAM panoramic cameras of Moonglow Technologies 24/7 monitor the skies above Aragats station. A one-minute time series of camera shots are available directly from the ADEI menu (from 2012). A circular fisheye system provides

a 190° hemispherical field of view. The image sensor is a Color 1/3" Sony Super HAD CCD II with an effective pixel number across FoV of 546×457 , with an automatic exposure time (from 10^{-5} to 4 s). In 2018, 2 additional cameras were installed on the roof of new small laboratory houses an electric mill and weather station. New laboratory is intended to host instruments from other parties for calibrated their airborne particle detectors with TGEs registered by Aragats facilities. We use cameras for observing transient luminous events coinciding with large TGEs, and the graupel falls by the characteristic specks on the camera glass.

The fast wideband electric field waveforms produced by lightning discharges are recorded with a

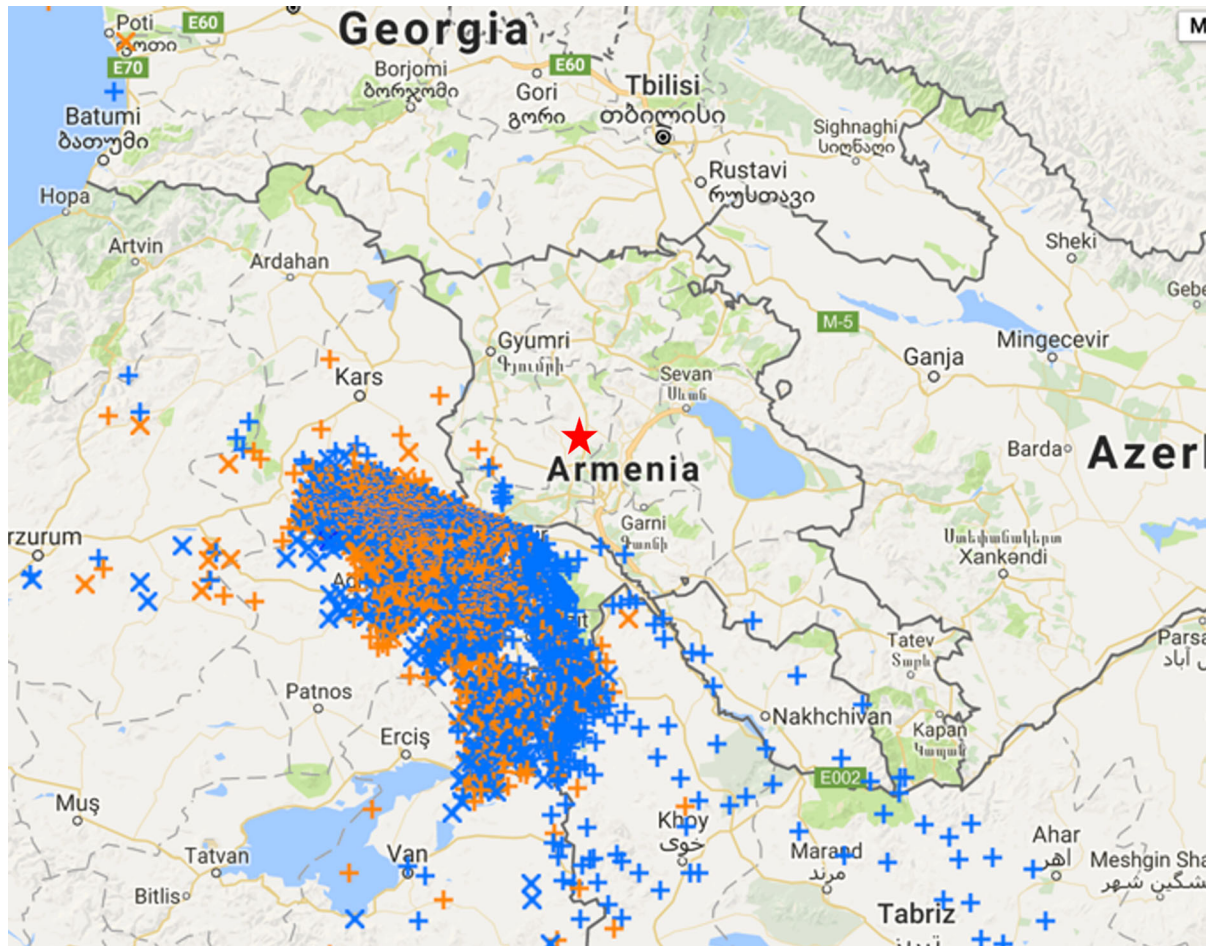


Figure 2

A thunderstorm is approaching Armenia from the southwest. Lightning flashes were located from 17:21 to 18:25 UT on 22 May 2018. Crosses are cloud-to-ground flashes, and pluses are intracloud flashes. Orange ones are normal polarity intracloud and positive cloud to ground, and blue ones are inverted polarity intracloud and negative cloud to ground. By red asterisk, we denote Aragats stations

circular flat-plate antenna followed by a passive integrator. The output of the integrator is connected via a 60 cm double-shielded coaxial cable to a Picoscope 5244B digitizing oscilloscope. The frequency bandwidth of the wideband electric field measuring system is 50 Hz to 12 MHz (the RC decay time constant is 3 ms). The record length is 1 s, including 200 ms pretrigger time and 800 ms post-trigger time. The sampling rate is 25 MS/s (sampling interval of 40 ns), and the amplitude resolution is 8-bit. The fast wideband electric field data from 2014 are stored on the ASEC servers and is available upon request.

Aragats measuring facilities are located inside and around 3 experimental halls on Aragats. Most of the particle detectors in 2009 were located in the MAKET experimental hall, Fig. 3. The Aragats Solar Neutron Telescope (ASNT, data available from 2003), which remains the largest spectrometer in HEPA research (4 m²), measures the flux of electrons and gamma rays in the energy range 10–100 MeV. In the same hall are the Aragats Neutron Monitor (ArNM, data from 2003), type 18HM64, the SEVAN particle detector and muon detector (data from 2008). 16 plastic scintillators of the MAKET-ANI surface array record both EASs and TGEs. A network of three STAND1 detectors (three stacked

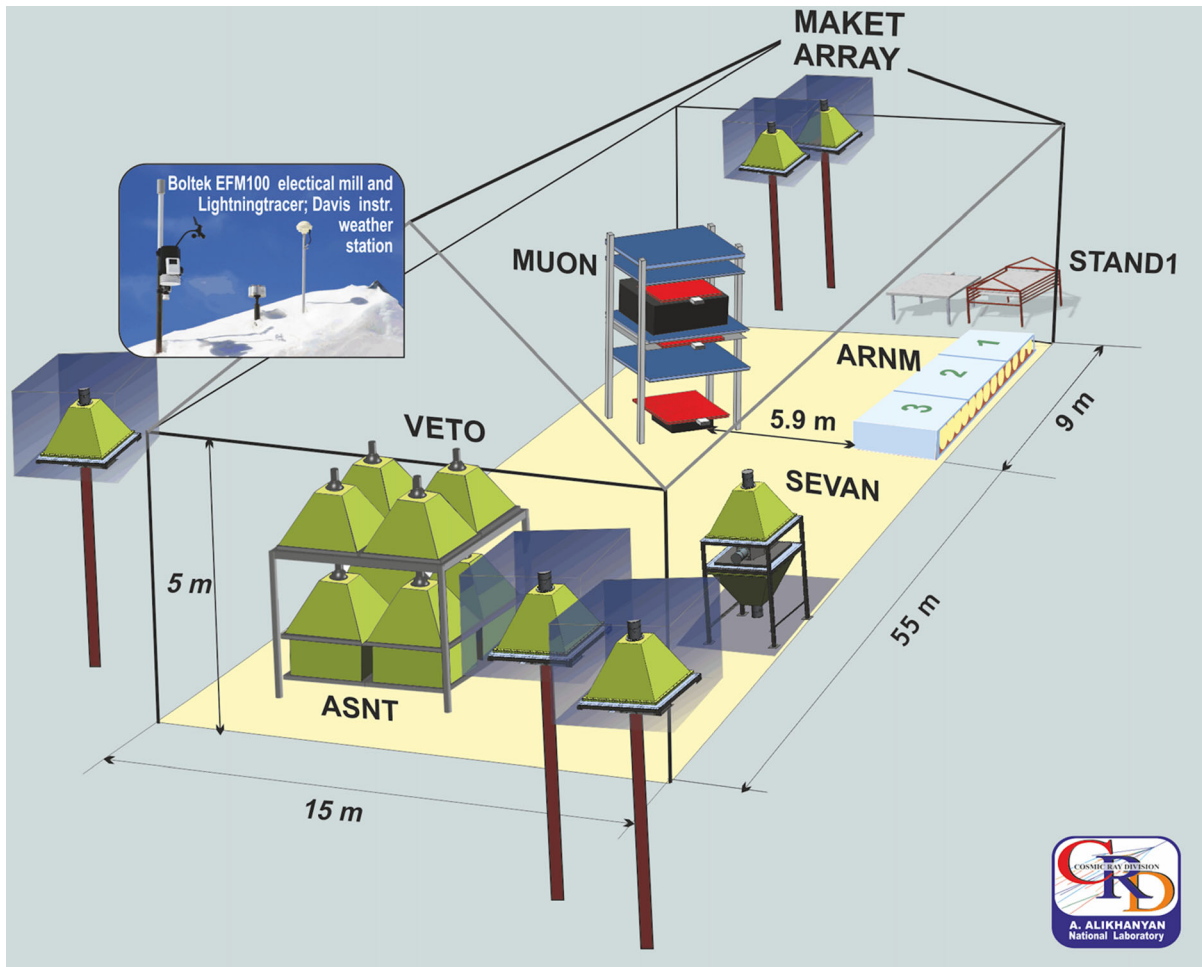


Figure 3
Measuring devices located in and near the MAKET experimental hall (description of facilities in the text)

scintillators with a thickness of 1 cm and an area of 1 m^2 and one stand-alone with a thickness of 3 cm) is located at Aragats station premises covering a $50,000 \text{ m}^2$ area; see one of the detectors under the west wall of MAKET building in Fig. 3. DAQ electronics based on National Instruments (NI) MyRIO board (see details in Chilingarian et al., 2024c) captured 50 ms time series from STAND1 network, which are available via ADEI from 2011. The electric field sensors, weather station, and all-sky camera are installed on the roof of the MAKET building.

A network of seven spectrometers (based on NaI crystals of $12 \times 12 \times 28 \text{ cm}$ size) are installed in the SKL experimental hall, see Fig. 4. The low energy threshold ($\sim 300 \text{ keV}$) provides large

statistics ($\sim 50,000$ counts per minute) for recovering the gamma-ray differential energy spectrum from 0.3 to 50 MeV (Chilingarian et al., 2022b). In the same hall are located particle detectors STAND3 and CUBE, the flat plate antenna, and digitizing oscilloscopes. Under the East wall of the building operates another STAND1 and CsI (TL) detectors; on the roof of the SKL building, interferometer antennas, and an EFM 100 electric mill are installed. For registration of the location of lightning discharges in Aragats, we use a short-baseline Very High Frequency (VHF) interferometer system (Chilingarian et al., 2020a). A four-channel Picoscope 6403D digitizing oscilloscope is used to capture the signals from the antennas. The maximum real-time sampling rate of the

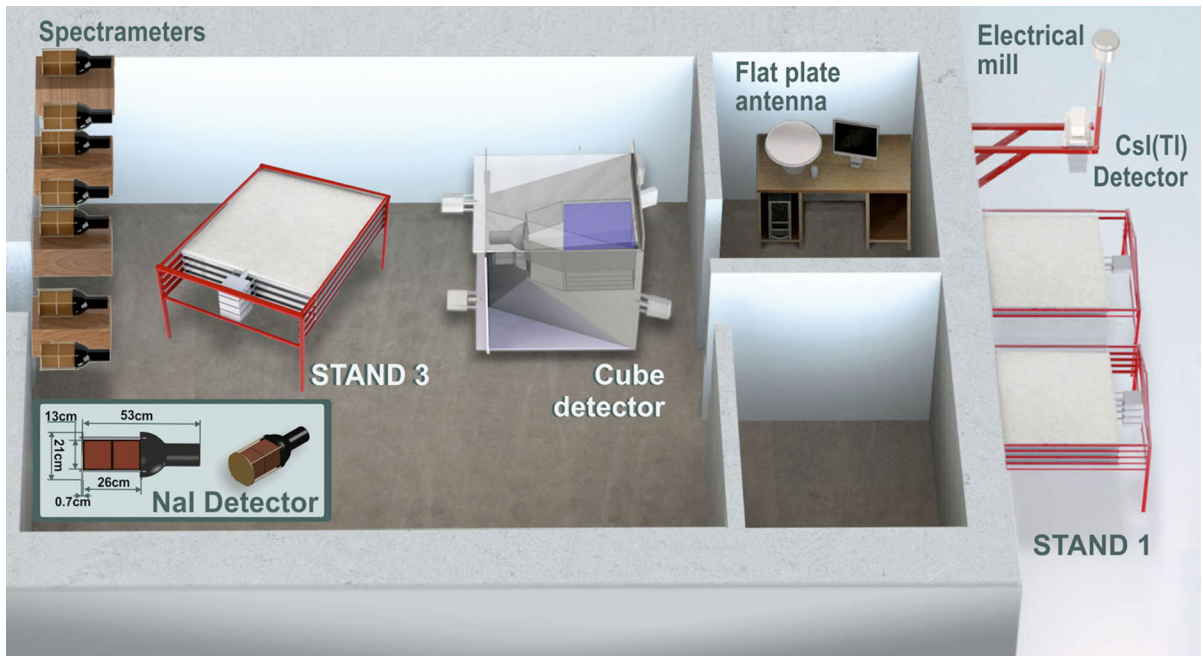


Figure 4

A schematic view of the SKL experimental hall and outside (description of facilities in the text)

oscilloscope is 5 GS/s (1.25GS/s for four-channel operation), and the memory depth is 1GS (250MS per channel). The interferometer operates in the frequency range from 24 to 78 MHz. It employs three circular flat-plate antennas of 30 cm diameter, which are located in the horizontal plane and form two orthogonal baselines of 13 m in length. The time differences of arrival of the signals at pairs of antennas determined from the peak of the cross-correlation function are used to measure the azimuth and elevation angles of the radiation source as a function of time. The interferometer data are digitized at 156.25 MS/s sampling rate (sample interval of 6.4 ns). Interferometer data starting from 2017 are available from (Interferometer, 2024).

The third STAND1 detector and electric mill are located at the GAMMA detector of the ANI experiment (Danilova et al., 1982); see Fig. 5. In the underground hall, a 200 m² muon detector is located, by which the maximum energy of solar proton accelerators was estimated to be above 20 GeV (Solar energetic event of 20 January 2005, Bostanjyan et al., 2007).

3. Advanced Data Extraction Infrastructure (ADEI)

The data mining, visualization, and statistical analysis of the big data coming from modern observatories, which study the high-energy phenomena in space and the atmosphere, have become an important tool in scientific research. Multivariate analysis of variations of fields, radiation, and particle fluxes can provide new information on the development of thunderstorms, including those of catastrophic nature. Such analysis presents a challenge due to the large quantity of acquired data. A huge amount of time series should be processed and identified in real-time for forecasting and alerts, as well as for reporting and paper preparation. Usually, researchers have no time to access archives if the data stream is pressing and new interesting events appear each new day. Therefore, to support researchers in data mining and finding “new physics,” a multivariate visualization platform should be supplemented with tools of elementary statistical analysis (histograms, moments, correlations, comparisons), figure preparation, and archiving, i.e., with data exploration system.

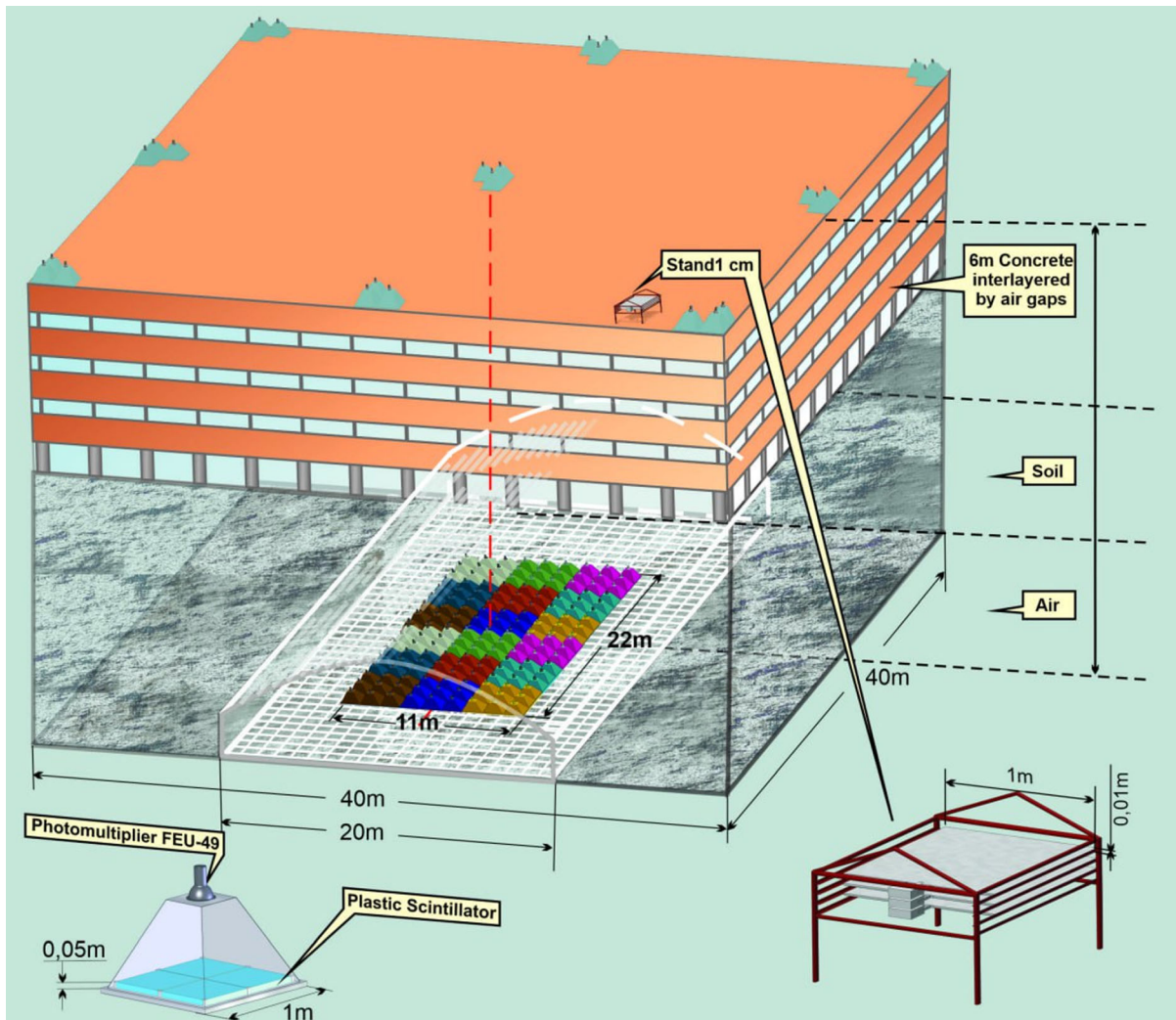


Figure 5

The calorimeter of the ANI experiment. The scintillators of the GAMMA array are located on the roof and in the underground hall (Garyaka et al., 2002). The third STAND1 detector and EFM 100 electric mill are located on the roof of the calorimeter and the roof of the scintillator housing

The ASEC's databases are open-access and contain multivariate measurements on hundreds of TGEs, including the time series of the electric field strength and records of particle fluxes and interferometer antenna signals. Methods for visualization and analysis of multidimensional experimental data are successfully used to study the solar-terrestrial connections and high-energy phenomena in the terrestrial atmosphere. ASEC provides access to all

historical data via ADEI, designed to offer multivariate visualization and data exploration capabilities for multiple remote measurements. Raw data is stored as CSV and XML files, processed by cron scripts and loaded into the MySQL database, integrated with the ADEI platform. The ADEI Wiki page provides all the necessary instructions and a description of data and sensors. Database operators need a tool to examine all collected data, checking the integrity and

validity of measurements. This tool is also needed to search for and export data possessing specified characteristics.

To provide such broad coverage, ADEI utilizes a highly modular architecture. The system consists of backend and frontend parts communicating over HTTP protocol using Asynchronous JavaScript and XML (AJAX; refer to software used by Chilingaryan et al., 2010) approach. The ADEI backend defines a few abstract interfaces to implement various capabilities using simple plugins. The data sources are interfaced with dedicated drivers and implemented as a data access abstraction layer. The higher system levels utilize this abstract interface to get data uniformly from arbitrary storage.

The Google Maps interface inspires the ADEI web frontend. Single or multiple time series are plotted using the data from the currently selected time interval. Then, the plot can be dragged and zoomed over time and investigated parameters. The desired region of the plotted variables may be selected for detailed statistical analysis or exported in one of the supported formats.

Data from local and international networks is transferred to the MySQL database at the CRD headquarters in Yerevan and is available through ADEI. The platform allows users to analyze data quickly, prepare figures and slides, perform joint data analysis with remote groups, test hypotheses, and draw physical inferences. Alerts and forewarnings sent by e-mail make it possible to follow the progress of solar and thunderstorm events in real time. ADEI database contains a time series of neutral and charged particle count rates together with data on disturbances of the NSEF measured by a network of Boltek EFM-100 electric field mills and meteorological conditions from automatic weather stations from Davis Instruments. Combining particle fluxes and environmental parameters in a single database enabled the visualization and multivariate correlation analysis, as well as the issuing of alerts for hazardous space weather events (Gevorgyan et al., 2005).

4. Coherent Measurements of Particles and Fields on Aragats Stations

Large-scale AEF accelerates and multiplies free electrons initiating avalanches reaching the Earth's surface and registered as impulsive enhancements of particle detector count rates. Direct and remote monitoring of AEF is not yet feasible on Aragats. Instead, we use its proxy—NSEF, measured with networks of electric mills, see Figs. 1, 3, 4. The ADEI provides continuous 1 s time series of NSEF measurements at fair weather and during thunderstorms since 2010, as well as distances to lightning flashes. In Fig. 6, we present data from a stormy day on Aragats started at noon UT, 4 PM local time (the difference between local time and UT in Armenia is constant and equals -4 h), and near Nor Amberd station at 2000 m height. In Nor Amberd, the NSEF was initially in the positive domain, rapidly reaching a value of 20 kV/m. It then decreased to 15 kV/m before changing polarity after a nearby lightning flash, causing it to become negative (-15 kV/m). After half an hour, the NSEF decayed to its fair weather value. Several lightning flashes caused sudden changes in the NSEF, increasing the charge above the ground (normal polarity intracloud flashes). To highlight the relationship between lightning and NSEF, we included a zoomed version of the time series in the inset on the bottom left corner of the figure. Storm after ceasing in Nor Amberd “climbed” to Aragats at 13:40. The NSEF was in the deep negative domain (-30 kV/m) that usually leads to RREA in the thundercloud and TGE on the ground.

In Fig. 7, we show the multivariate information gathered for analyzing a developing TGE. We aim to get insight into the emergence of the charge structures in the cloud, which accelerate seed electrons from the ambient population of cosmic rays up to 50 MeV. As we can see in Fig. 7e, the upper 5 cm thick and 1 m² area plastic scintillator of the SEVAN detector (Chilingarian et al., 2018) registered an unprecedentedly long TGE lasting from 13:45 to 14:20 (usually the lightning flash “kills” TGE after a

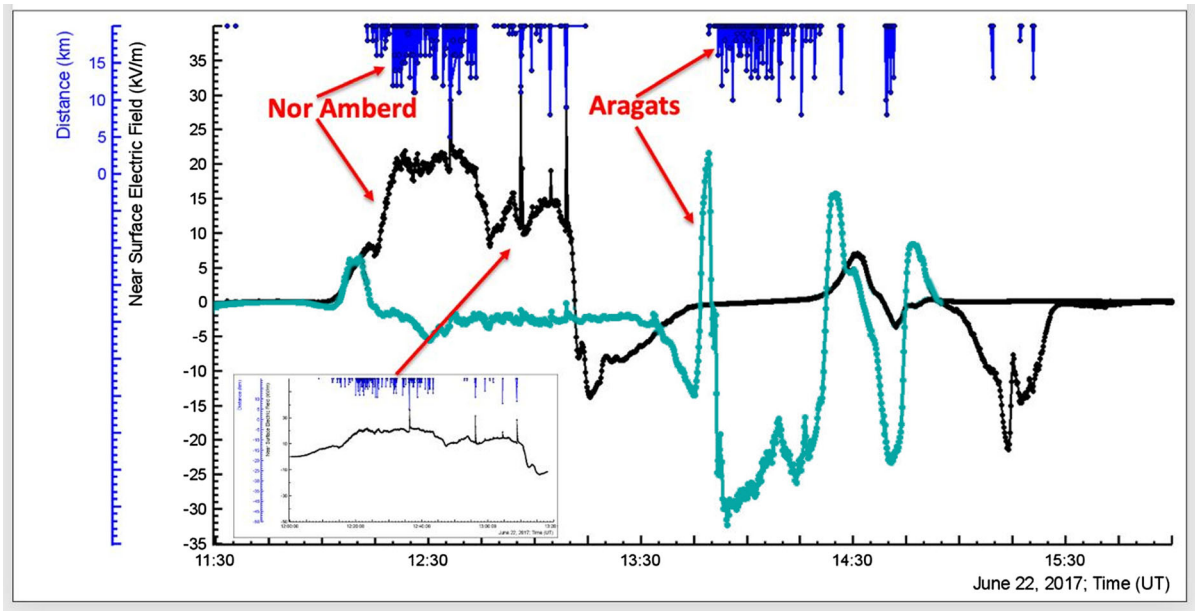


Figure 6

The one-second time series of the NSEF measured at Nor-Amberd (black curve) and Aragats (aquamarine). The inset shows a zoomed version of the Nor-Amberd storm. Distances to lightning flashes are shown in blue at the top of the figure

few minutes) when NSEF was in the deep negative domain. At $\approx 14:00$, we notice a brief outburst of NSEF up to 10 kV/m coinciding with a quick rise of the particle flux. Positive NSEF indicates the emergence of the lower positively charged region (LPCR, Chilingarian & Mkrtchyan, 2012). The dipole between the negatively charged main negative region (MN) and LPCR effectively accelerates electrons starting RREA, which is indicated by the quick rising count rate of the particle detector. LPCR is a transient structure “sitting” on the graupel hydrometeors and eliminated with the graupel fall. After LPCR diminished with graupel fall, a dipole emerged between NM and its mirror in the ground, continuing the initiation of RREAs in the large-scale AEF. The indication of LPCR ceasing is the conical graupel fall at 13:45–14:20 (see Fig. 7b–d), observed by all-sky cameras and confirmed by a photo made by the station staff. In Fig. 7a, we show a time series of the cloud base height recovered by the difference between the outside temperature and dew point (the so-called spread). Thus, the multisensory observation of the storm helps to join all measurements in the comprehensive explanation of the TGE phenomenon.

All figures (including sky shots) are generated by ADEI and then composed in MS PowerPoint slides.

The procedure of selecting detectors for the multivariate analysis and corresponding times is rather simple, explained in the Wiki section of ADEI. Users must select time and sensors in the user-friendly menu in the ADEI left panel. The number of time series in the figure is not limited; each measurement has its color and Y-axes. The time series can also be plotted in percent and a number of mean-standard deviations relative to the fair-weather value measured before the TGE (the first 1/3 of horizontal time axes). In the left menu, statistical analysis tools can be selected, like the calculated spread shown in Fig. 7a). By selecting the scale for each measurement, the time series with different colors can be positioned in the Figure. This feature is very convenient for visualizing the relation between variables, for instance, how the TGE depends on NSEF. Scatter plots, histograms, delayed correlation analysis, and other statistical procedures are available. Plots can be automatically stored, and data in CVS and MS EXCEL formats can be exported.

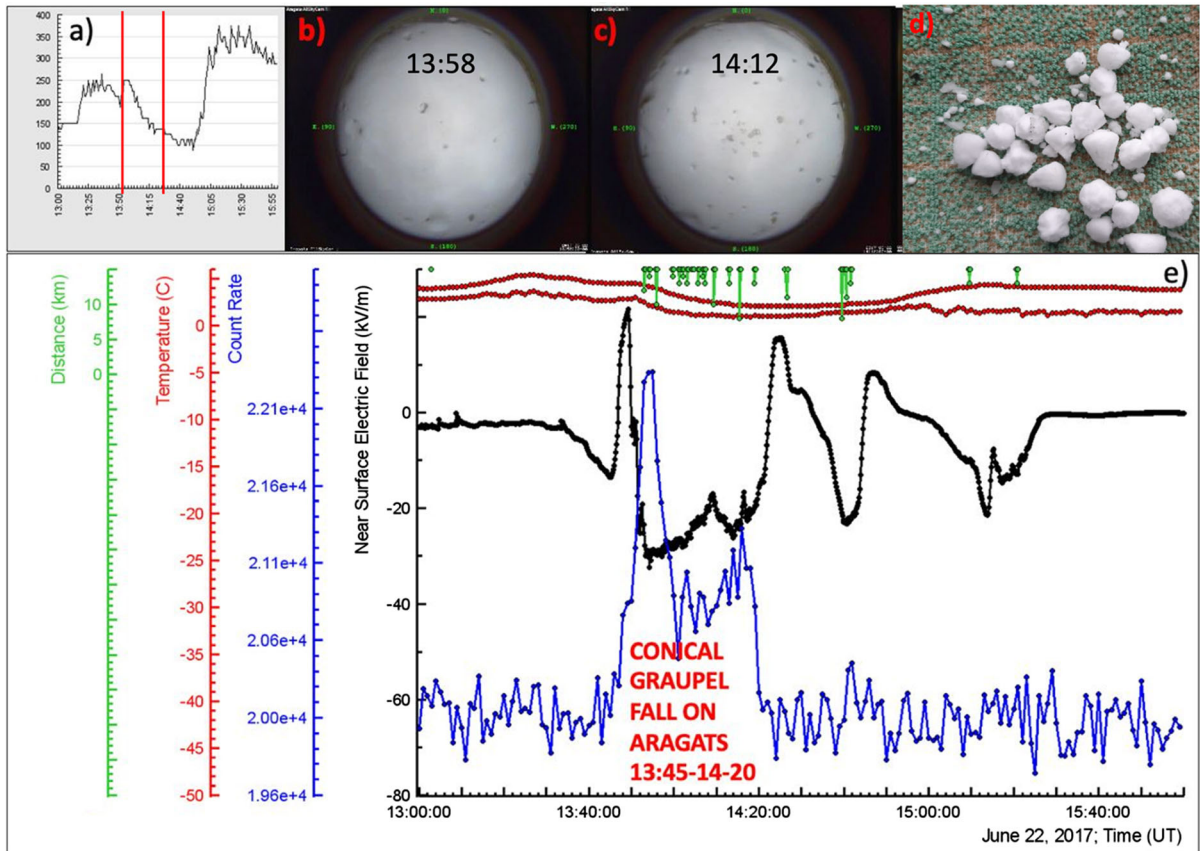


Figure 7

a The time series of distances to the cloud base; **b, c** the panoramic camera shots when the thick cloud was “sitting” on the station, the spots on the camera glass; **d** photography of the open sky above the station after the storm decays; **e** black—the NSEF disturbances, blue—the 1-min time series of particle fluxes, red—the outside temperature and dew point, green—distances to the lightning flash. By red lines in **a**, we denote TGE time

Figures 8 and 9 present one-second time series of the count rates of 1 m² area scintillators of the STAND1 network observing a large TGE. The network comprises three detectors covering a 50,000 m² area at Aragats station (Chilingarian et al., 2022a). The blue curves represent the count rates, while the black curves represent the disturbances of the NSEF, which diminished to -20 kV/m at TGE’s maximum. The red lines indicate the distances to the nearest lightning flash. It’s worth noting that lightning activity within 15 km was absent. The scatter plot in the inset emphasizes the relation between lowering NSEF and the rising flux of the TGE.

The count rate during 30 s of TGE maximums significantly exceeded the count rate measured during

fair weather. On October 16th, the increase was 253%, corresponding to 11.3 standard deviations above the mean count rate measured during fair weather. On November 6th, the increase was even larger at 350%, with a significance level of 17.8 standard deviations. It has been observed that the uniform flux of particles remains consistent across an area of approximately 50,000 square meters covered by the STAND1 network (Chilingarian et al., 2024c). What is noteworthy about this observation is the perfect correlation between the rising TGE flux and the diminished NSEF (a proxy for the atmospheric electric field), as shown in the insets of pictures 8 and 9. Thus, this is the first evidence demonstrating that the intensity of the electron “beam” in the

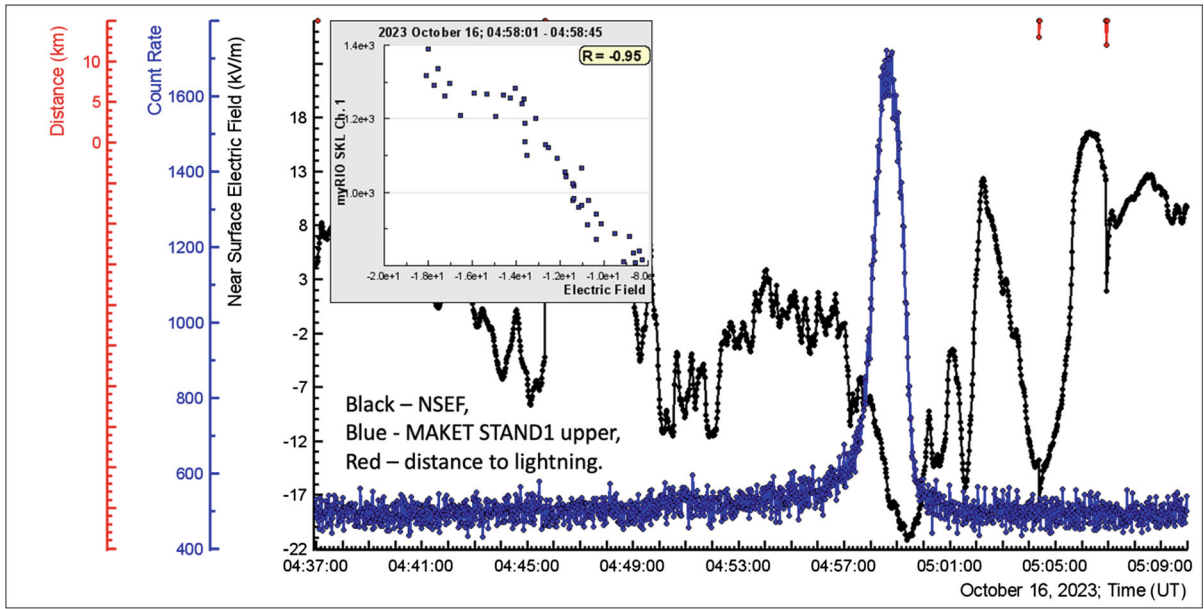


Figure 8

1 s time series of disturbances of NSEF (black curve) and count rate of 1 m² area 1 cm thick upper scintillator of the outdoor STAND1 network. Red lines denoted distances to the lightning flashes. The inset shows a scatter plot between rising particle flux and NSEF

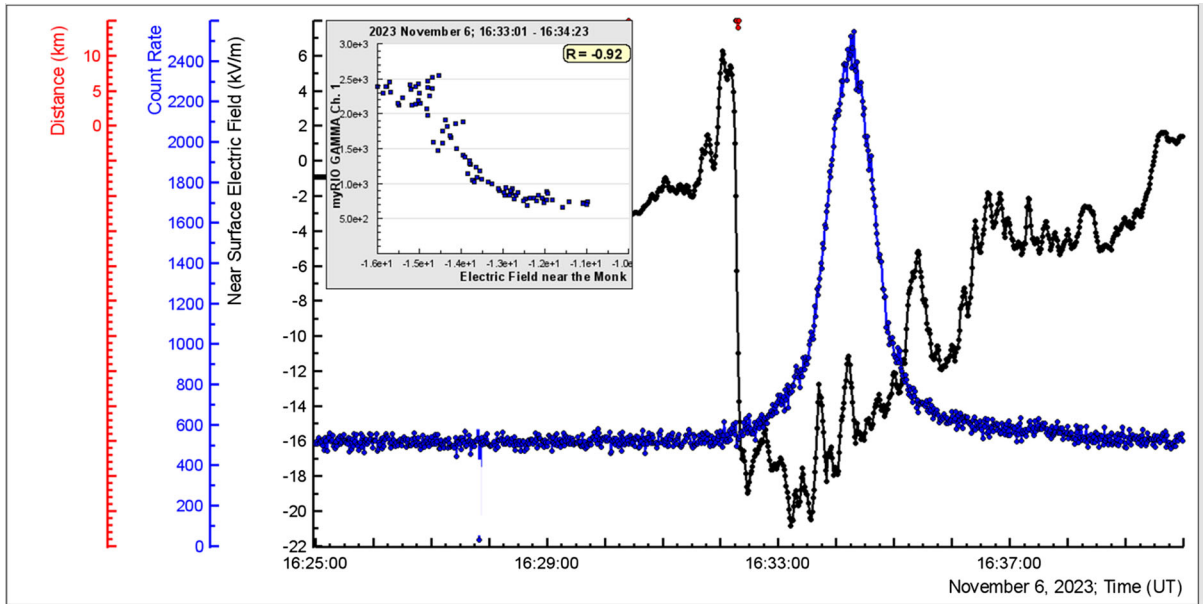


Figure 9

1 s time series of disturbances of NSEF (black curve) and count rate of 1 m² area 1 cm thick upper scintillator of the outdoor STAND1 network. Red lines denoted distances to the lightning flashes. The inset shows a scatter plot between rising particle flux and NSEF

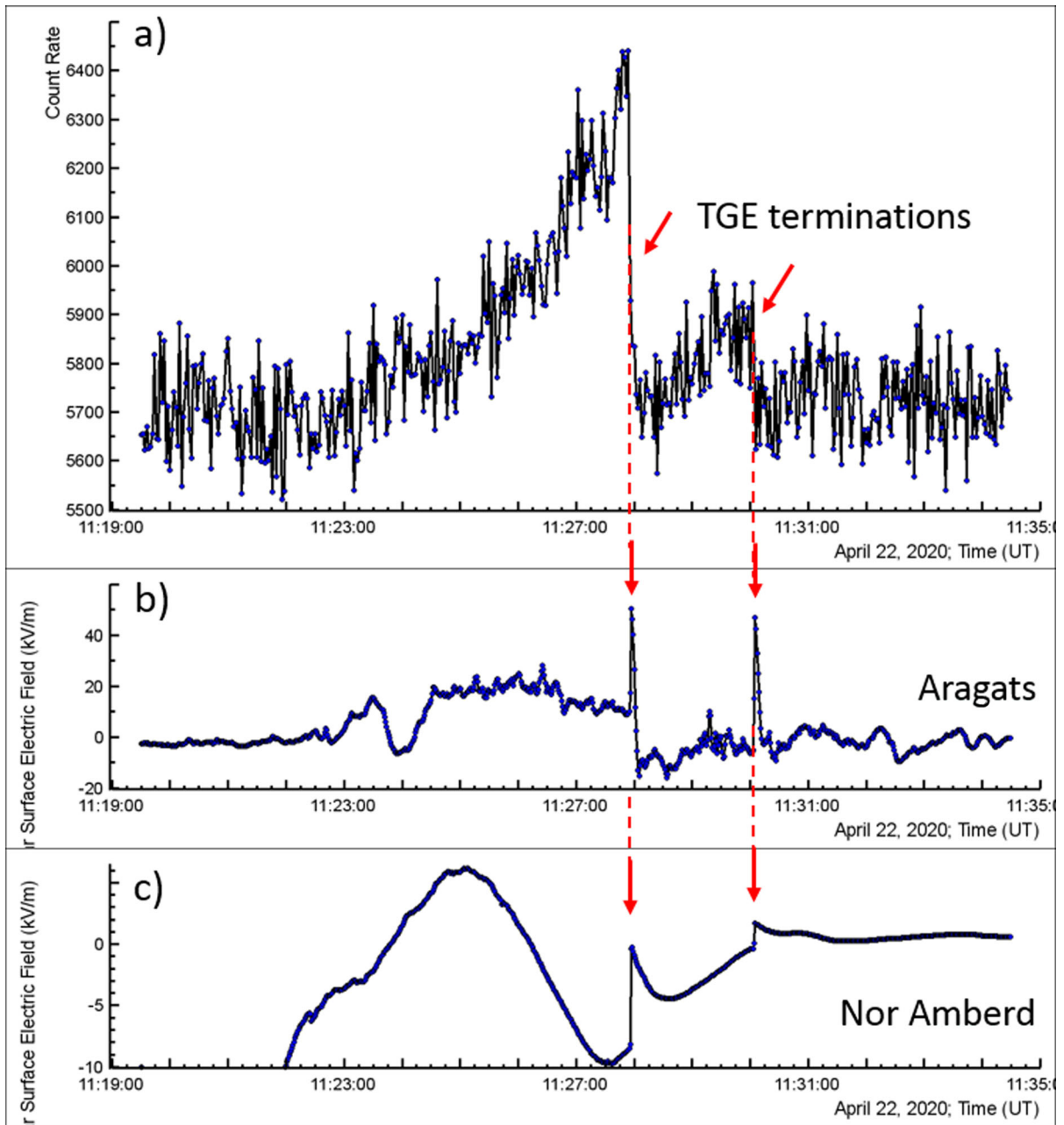


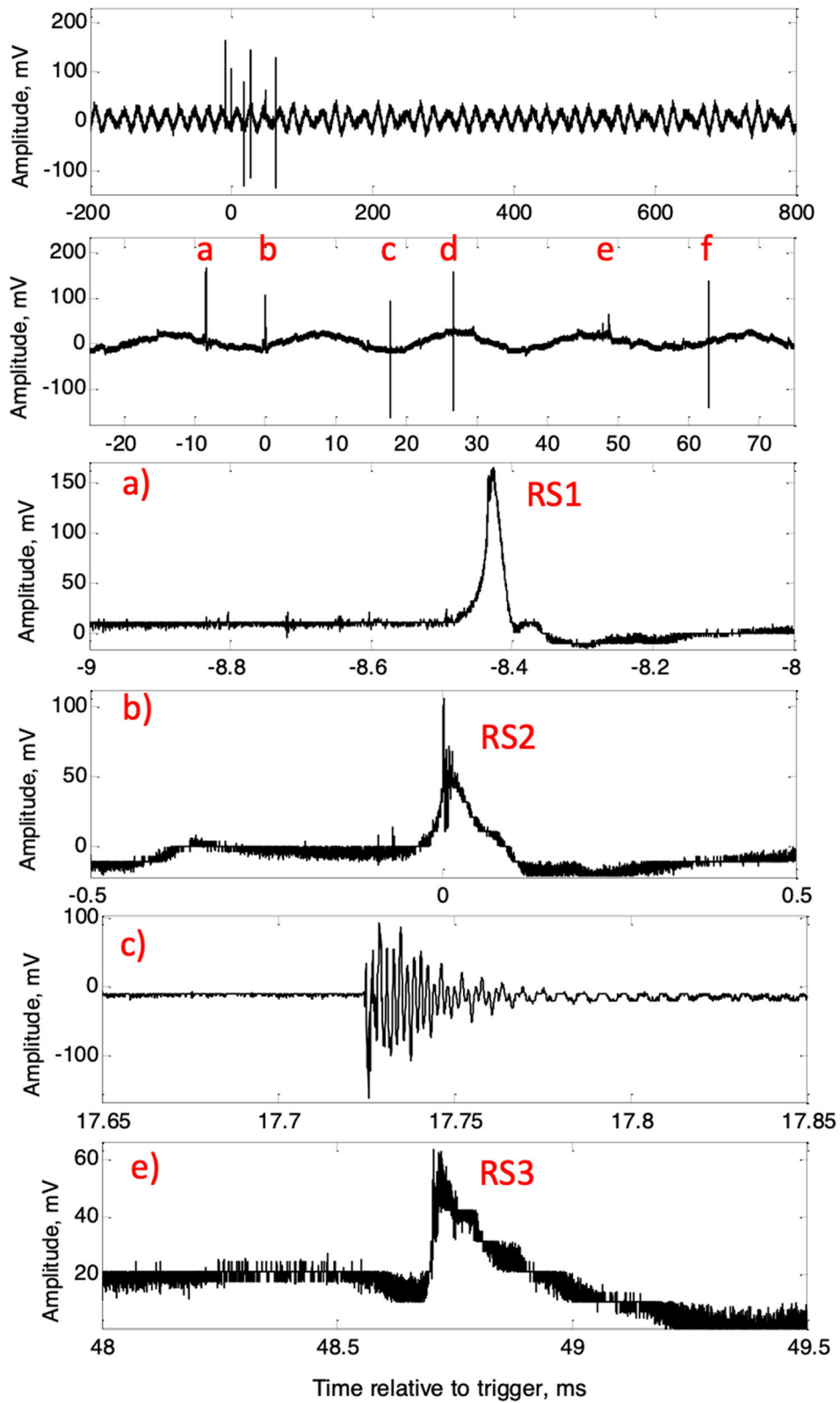
Figure 10

Particle flux at Aragats (a) and electrostatic field changes recorded by field mills at Aragats (b) and at Nor Amberd (c) (separated by 12.8 km). Two lightning flashes terminated TGE at 11:27:56.719 UT (N1) and 11:30:04.561 UT (N2) on April 22, 2020

atmosphere is directly proportional to the strength of the electric field between the mean negative layer in the middle of the cloud and the Earth's surface.

5. TGE Termination by Lightning Discharges

Next, we will examine two events of TGE termination by lightning flash observed at Aragats station during the Spring–Summer 2020. We analyze



◀Figure 11

A fast wideband electric field record of negative CG occurred at 11:27:56.719 UT on April 22, 2020 (flash N1), shown on different time scales. Signatures indicated by c, d, and f in panel 2 have similar shapes

the signal from the particle detector, the NSEF measured by the field mills at Aragats and Nor Amberd, and the fast wideband electric field (E) record. For one of the events, we also demonstrate observations of the lightning discharge by the VHF interferometer (Chilingarian et al., 2020a). We use the methodology developed in our earlier studies by Chilingarian et. al. (2017b, 2020c) for lightning-type classification. We classify lightning types assuming the well-known tripolar model of the normal-polarity thundercloud charge structure. Classification methodology includes the following main steps:

1. First, we check the polarity of electrostatic field change ΔE at the Aragats station, which is always the closest to the lightning flash in this study. If $\Delta E > 0$, the flash is classified as either $-CG$ or normal-polarity IC that occurred within the reversal distance of the Aragats station. If $\Delta E < 0$, the flash is classified as $+CG$ or inverted-polarity IC that occurred within the reversal distance of the Aragats station.
2. Next, to resolve the ambiguity between CGs and ICs, we check if the polarity of electrostatic field change ΔE reverses with distance, additionally using our remote field mills (usually the one at Nor Amberd). Polarity reversal of electric field change with distance can occur only for cloud discharges, while the polarity of electric field changes produced by CGs is always independent of distance
3. To distinguish between ICs and CGs or hybrid flashes (IC followed by CG), we analyze fast wideband electric field records to search for characteristic return stroke (RS) signatures. Since RS occurs only due to lightning contact with the ground, RS signatures indicate CGs. If at least one RS signature is found, but ΔE reversed with distance, the flash is identified as a hybrid.

On April 22, 2020, strong TGE was interrupted by a lightning flash at 11:27:56.719 (flash N1, $-CG$), and the second flash (N2) of the same type occurred at 11:30:04.561 stopped the attempt to restart the operation of the electron accelerator. Particle flux and the NSEF changes separated by ~ 2 min are shown in Fig. 10. The particle flux measured at Aragats by the 60-cm detector (2-s time series) is shown in panel (a), and electrostatic field measured at Aragats and Nor Amberd (1-s time series) are shown in panels (b) and (c), respectively. For each of the two lightning flashes, the sudden electric field change caused by the lightning discharge leads to an abrupt reduction of the particle flux. As seen from panels (b) and (c) in Fig. 10, the electrostatic field changes detected by two field mills at Aragats and at Nor Amberd have the same positive polarity for both flashes, that is, polarity reversal of electrostatic field change with distance is not detected. Therefore, they can be either a negative cloud-to-ground flash ($-CG$) or a normal intracloud ($+IC$) flash. To distinguish between CG and IC, we examine fast wideband electric field (E) records where we search for characteristic return stroke (RS) signatures.

Figures 11 and 12 show E field records produced by flash N1 and N2, respectively. As seen from panels (a, b, and e) in Fig. 11 and panels (b and c) in Fig. 12, the E field records for both flashes contain relatively wide positive polarity pulses. The rise times of these two pulses are about 5–10 μs , and the peak-to-zero fall times are 20–150 μs . We attribute these two pulses to return strokes of negative cloud-to-ground ($-CG$) lightning. It is worth noting that flash N1 was also detected by the worldwide lightning location network (WWLLN), one of the nodes located in Yerevan. Thus, both lightning flashes that terminated the TGE (Fig. 10) can be classified as $-CG$.

Another strong TGE was terminated by an inverted IC followed by $-CG$ on June 21, 2020, at 11:03:51.906 UT. Figure 13 shows the effect of lightning flash on the enhanced particle flux observed at 11:03:51.906 UT on June 21, 2020. An abrupt decrease in particle count rate (panel a) is observed during a fast negative NSEF change in Aragats. As seen from panels (b) and (c) in Fig. 14, polarity reversal of electrostatic field change ΔE with distance

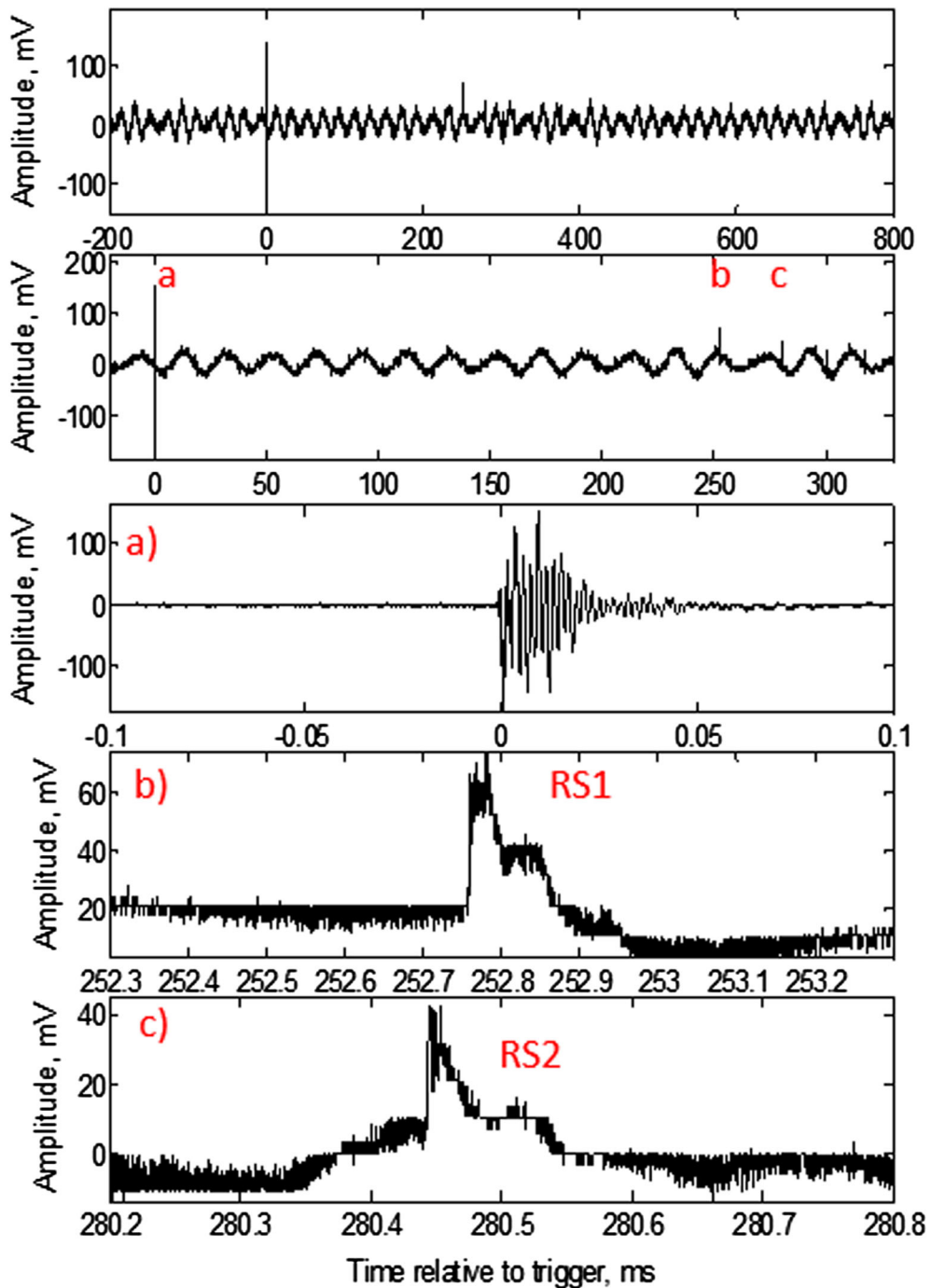


Figure 12

A fast wideband electric field record of negative CG occurred at 11:30:04.561 UT on April 22, 2020 (flash N2), and it is shown on different time scales

is detected: ΔE is negative (large) in Aragats and positive (small) in Nor Amberd. A larger change in

the electrostatic field corresponds to a smaller distance to the lightning. The observed behavior of

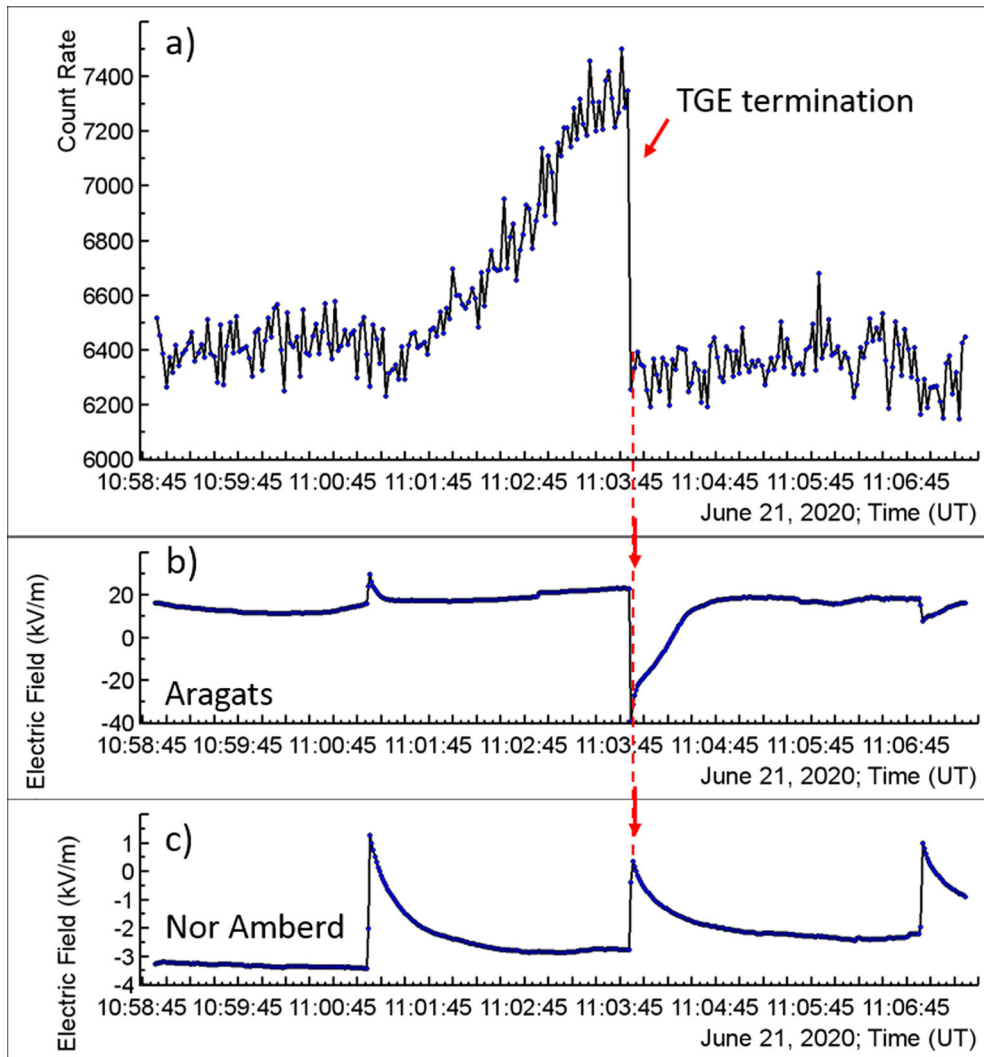


Figure 13

Particle flux at Aragats (a) and electrostatic field changes recorded by field mills at Aragats (b) and at Nor Amberd (c) for TGE-terminating lightning flash that occurred at 11:03:51.906 UT on June 21, 2020

electrostatic field change indicates that this lightning discharge partially destroyed a vertical negative dipole (negative charge above positive). The negative polarity of an electrostatic field change (larger field change in Aragats) is determined by the dominant contribution from the neutralization (complete or partial) of the lower positive charge region (LPCR). The contribution of reducing the higher-altitude negative charge is dominant at the larger distance in Nor Amberd, where the NSEF change is positive.

Thus, one could classify this lightning as an inverted IC, which occurs between the mid-level negative charge region and the LPCR. However, examination of the fast wideband electric field record (Fig. 14) reveals return stroke (RS) signatures indicative of $-CG$. As seen from Fig. 14, cloud discharge pulses in panel (a) are followed by five return strokes shown in panels (b, c, d, and e). Thus, even though an elevated negative dipole is neutralized, this discharge cannot be classified as a “pure” inverted IC flash. Notably, the polarity of five return

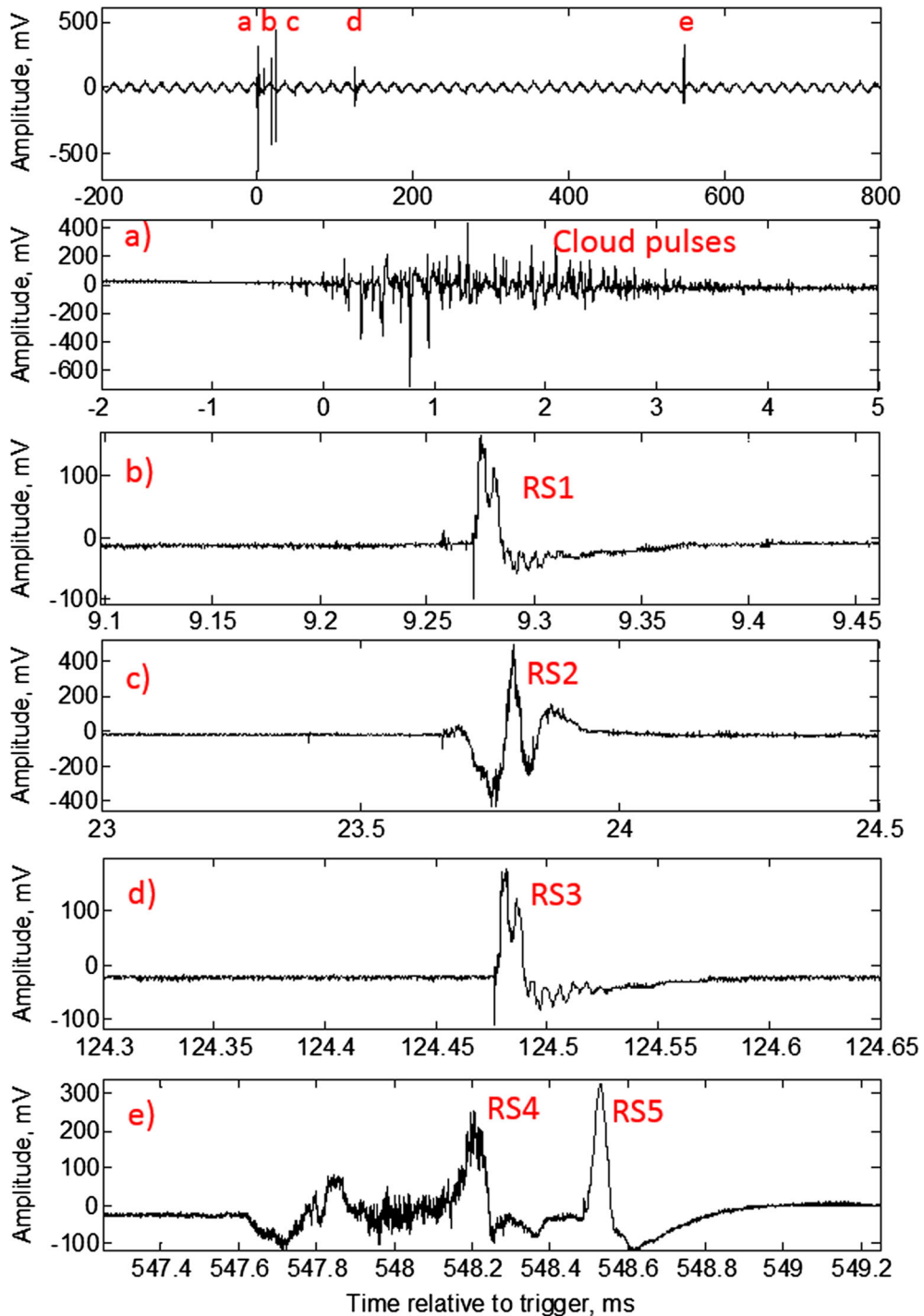


Figure 14

Fast wideband electric field record of lightning flash that occurred at 11:03:51.906UT on June 21, 2020, shown on different time scales

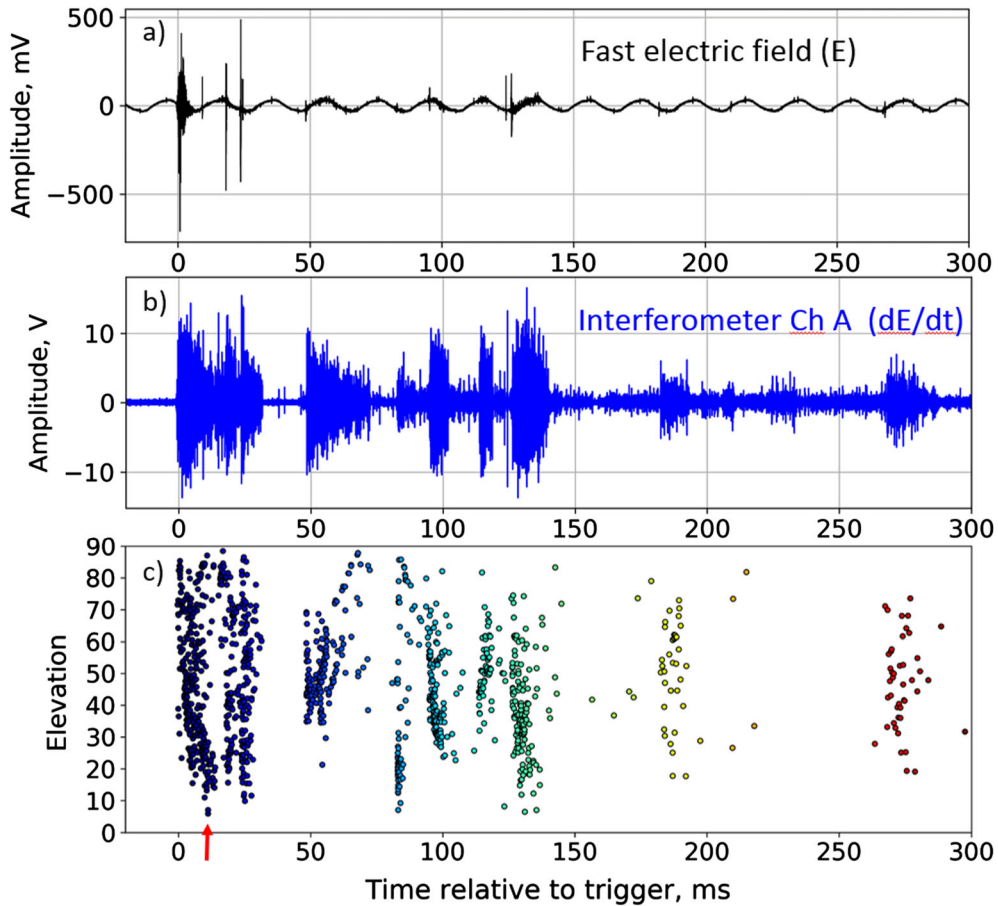


Figure 15

Record of wideband electric field (a), interferometer record (b), and elevation angle versus time (c) obtained by processing interferometer data for hybrid lightning that occurred at 11:03:51.906 UT on June 21, 2020. The red arrow indicates the time position of one of the return stroke pulses (RS₂) shown in panel c in Fig. 9

stroke pulses is positive, corresponding to removing the negative charge from the cloud and its transfer to the ground. We classify this event as a hybrid lightning flash when a $-CG$ lightning follows an inverted IC flash. Lightning flashes of this type were examined by Nag and Rakov (2009), Coleman et. al. (2008), Lu et. al. (2012).

We will now discuss the interferometer observations made during the lightning that occurred on June 21, 2020, at 11:03:51.906. Figure 15 shows synchronized records of wideband field and interferometer antenna signal (one of three channels), as well as the elevation angle versus time obtained by processing of interferometer data for hybrid lightning (inverted IC followed by $-CG$) that occurred at

11:03:51.906 UT on June 21, 2020. The signal of the fast wideband electric field in panel (a) is proportional to the electric field E , whereas the signal of the interferometer antenna shown in panel (b) is proportional to the time derivative of the electric field dE/dt . The records are shown for the time interval from -10 to 300 ms relative to the trigger.

Interferometric measurements allow us to get angular images of different stages of lightning discharge. For example, Fig. 16 shows an image of the lightning flash for a time interval from 10 to 27 ms relative to the trigger when the second return stroke pulse RS₂ at ~ 23.75 ms was detected (panel c in Fig. 15). The red arrow indicates the position of this interval in Fig. 16. The image is shown in rectangular

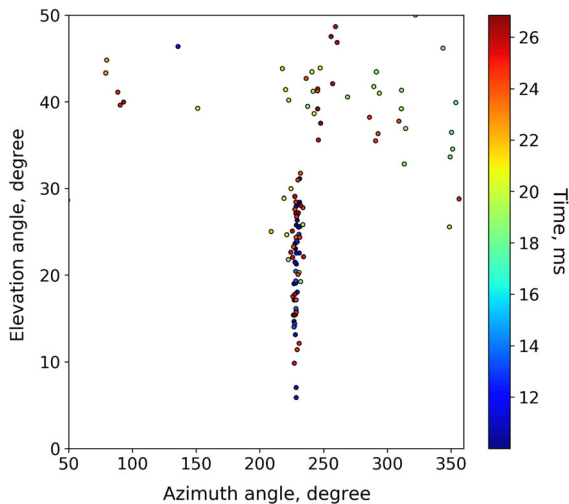


Figure 16

Elevation versus azimuth plot for hybrid lightning occurred at 11:03:51.906 UT on June 21, 2020. The time interval is from 10 to 27 ms relative to the trigger. Color coding indicates time

coordinates, where the azimuth angle is plotted on the horizontal axis. The elevation angle is on the vertical axis. As seen in Fig. 16, this cloud-to-ground discharge of a hybrid lightning flash occurred at an azimuth angle of 225° . Identification of this part of hybrid lightning as a -CG discharge is confirmed by the observation that the minimum value of the elevation angle is about 6° ; that is, the discharge propagates practically up to the horizon and strikes the ground.

Considered examples demonstrate that synchronous measurements of fast wideband electric field waveforms and the near-surface electrostatic field produced by lightning, complemented by interferometer observations, make it possible to identify the type of lightning flash. Combined analysis of fast wideband field waveforms and interferometer data provides useful information on various signatures in the waveform corresponding to different stages of lightning discharge. Termination of TGEs by lightning discharge indicates their association with the electric field produced by the thundercloud.

6. Conclusions

We present Aragats Space Environmental Center (ASEC) facilities aimed of researching high-energy

physics phenomena in the terrestrial atmosphere. To acquire the expected new knowledge, data samples from the measurements of slow and fast electric fields and elementary particle fluxes are combined to make a multivariate correlation analysis possible. Using the “electric” information and information on particle fluxes from electron accelerators operating in thunderclouds, we get insight into the emergence of the thundercloud charge structures, which enable the acceleration of seed electrons from an ambient population of cosmic rays up to 50 MeV. We demonstrate which charge structures supported RREA development and how to define the lightning type terminating TGE. For the first time, we show the exact correlation between the lowering absolute value of NSEF and rising particle flux. Observed synchronized records of wideband field and interferometer antenna signals, allowing us to get angular images of different stages of lightning discharge and connect the operation of the electron accelerators in thunderclouds with atmospheric electric field surges and lightning initiation (Chilingarian et al., 2017a).

The developed methodology realized in the ADEI multivariate analysis platform provides tools and services to integrate a multitude of space and geophysical observations into a system that fully utilizes the scientific potential of current geophysical observations. We demonstrate how to apply ADEI procedures for analysis and physical inference in HEPA experiments. With the growing archives of the time series from monitoring the various cosmic ray fluxes and atmospheric electric fields at ASEC and SEVAN, establishing a new infrastructure for correlating the data from numerous sources becomes increasingly urgent. The ADEI statistical modules and possibilities of multivariate visualization meet the needs of physical inference in multisensory, multidimensional environments.

ADEI is also used for Space Weather and Solar physics research, and we can present a set of ADEI layouts for physical inference in these domains. Physicists of the Cosmic Ray division prepared and published more than 80 articles heavily using the ADEI platform from 2013 to 2024 in high-rank scientific journals. ADEI tools make analytical work on sophisticated problems rather easy; one can try and

test many hypotheses very fast and come to a definite conclusion, allowing crosscheck and validation.

Acknowledgements

We sincerely thank the Aragats Space Environmental Center staff for their seamless operation of experimental facilities on Mount Aragats. We also thank A. Kiselyov for creating the interferometer software, and S. Soghomonian and V. Rakov for developing methods of joint analysis of particle fluxes and lightning discharges. S. Soghomonian performed the analysis of lightning flashes and wrote Sect. 5. This research effort was supported by the Science Committee of the Republic of Armenia, Research Project No. 21AG-1C012.

Author Contributions A.A.—supervision, methodology, manuscript writing, data visualization K.T.—data curation, resources, formal analysis B.S.—software, validation, investigation S.C.—database software, conceptualization Y.K.—methodology, formal analysis.

Funding

This study was supported by State Committee of Science of the Republic of Armenia (Grant No. AG-1C012).

Data Availability

The data underpinning this study can be accessed in numerical and graphical formats through the multi-variate visualization software platform ADEI, hosted on the Cosmic Ray Division (CRD) webpage of the Yerevan Physics Institute (ADEI, 2024).

Declarations

Conflict of Interest The authors declare no competing interests.

Publisher's Note Springer Nature remains neutral with regard to jurisdictional claims in published maps and institutional affiliations.

Springer Nature or its licensor (e.g. a society or other partner) holds exclusive rights to this article under a publishing agreement with the author(s) or other rightsholder(s); author self-archiving of the accepted manuscript version of this article is solely governed by the terms of such publishing agreement and applicable law.

REFERENCES

- ADEI. (2024). Retrieved January 1, 2024, from <http://adei.crd.yerphi.am/>
- Alexeenko, V. V., Khaerdinov, N. S., Lidvansky, A. S., et al. (2002). Transient variations of secondary cosmic rays due to atmospheric electric field and evidence for pre-lightning particle acceleration. *Physics Letters A*, 301, 299–306. [https://doi.org/10.1016/S0375-9601\(02\)00981-7](https://doi.org/10.1016/S0375-9601(02)00981-7)
- Auger, P., Ehrenfest, P., Maze, R., et al. (1939). Extensive cosmic-ray showers. *Reviews of Modern Physics*, 11(3–4), 288–291. <https://doi.org/10.1103/RevModPhys.11.288>
- Babich, L. P., Donskoy, E. N., Kutsyk, I. M., et al. (2001). Comparison of relativistic runaway electron avalanche rates obtained from Monte Carlo simulations and from kinetic equation solution. *IEEE Transactions on Plasma Science*, 29(3), 430. <https://doi.org/10.1109/27.928940>
- BOLTEK1. (2024). Retrieved January 1, 2024, from https://www.boltek.com/EFM-100C_Manual_030323.pdf
- BOLTEK2. (2024). Retrieved January 1, 2024, from <https://www.boltek.com/product/ld350-long-range-detection-kit>
- Bostanjyan, NKh., Chilingarian, A. A., Karapetyan, G., et al. (2007). On the production of highest energy solar protons on 20 January 2005. *Advances in Space Research*, 39, 1456–1459. <https://doi.org/10.1016/j.asr.2007.03.024>
- Chilingarian, A. (2024). Extensive air showers and atmospheric electric fields. Synergy of space and atmospheric particle accelerators. *JASR*. <https://doi.org/10.1016/j.asr.2024.03.013>
- Chilingarian, A., Babayan, V., Karapetyan, T., et al. (2018). The SEVAN worldwide network of particle detectors: 10 years of operation. *Advances in Space Research*, 61, 2680. <https://doi.org/10.1016/j.asr.2018.02.030>
- Chilingarian, A., Chilingaryan, S., Karapetyan, T., et al. (2017a). On the initiation of lightning in thunderclouds. *Scientific Reports*, 7, 1371. <https://doi.org/10.1038/s41598-017-01288-0>
- Chilingarian, A., Daryan, A., Arakelyan, K., Hovhannisyanyan, A., Mailyan, B., Melkumyan, L., & Hovsepian, G. (2010). Ground-based observations of thunderstorm-correlated fluxes of high-energy electrons, gamma rays, and neutrons. *Physical Review D*, 82, 043009. <https://doi.org/10.1103/PhysRevD.82.043009>
- Chilingarian, A., Dolgonosov, M., Kiselyov, A., Khanikyantsa, Y., & Soghomonian, S. (2020a). Lightning observations using broadband VHF interferometer and electric field measurements. *Journal of Instrumentation*, 15, P07002. <https://doi.org/10.1088/1748-0221/15/07/P07002>
- Chilingarian, A., Gharagyozyan, G., Hovsepian, G., Ghazaryan, S., Melkumyan, L., & Vardanyan, A. (2004). Light and heavy cosmic-ray mass group energy spectra as measured by the MAKET-ANI detector. *Astrophysical Journal*, 603, L29–L32.

- Chilingarian, A., Hovsepyan, G., & Hovhannisyanyan, A. (2011). Particle bursts from thunderclouds: Natural particle accelerators above our heads. *Physical Review D*, *83*, 062001. <https://doi.org/10.1103/PhysRevD.83.062001>
- Chilingarian, A., Hovsepyan, G., Karapetyan, T., et al. (2020b). Structure of thunderstorm ground enhancements. *Physical Review D*, *101*, 122004. <https://doi.org/10.1103/PhysRevD.101.122004>
- Chilingarian, A., Hovsepyan, G., Karapetyan, T., et al. (2022a). Multi-messenger observations of thunderstorm-related bursts of cosmic rays. *JINST*, *17*, P07022. <https://doi.org/10.1088/1748-0221/17/07/P07022>
- Chilingarian, A., Hovsepyan, G., Karapetyan, T., Sarsyan, B., & Chilingaryan, S. (2022b). Measurements of energy spectra of relativistic electrons and gamma-rays avalanches developed in the thunderous atmosphere with Aragats solar neutron telescope. *Journal of Instrumentation*, *17*, P03002. <https://doi.org/10.1088/1748-0221/17/03/P03002>
- Chilingarian, A., Hovsepyan, G., Khanikyanc, Y., Reymers, A., & Soghomonyan, S. (2015). Lightning origination and thunderstorm ground enhancements terminated by the lightning flash. *Europhysics Letters*, *110*, 49001. <https://doi.org/10.1209/0295-5075/110/49001>
- Chilingarian, A., Hovsepyan, G., Melkumyan, L., et al. (2007). Study of extensive air showers and primary energy spectra by MAKET-ANI detector on Mountain Aragats. *Astroparticle Physics*, *28*, 58–71. <https://doi.org/10.1016/j.astropartphys.2007.04.005>
- Chilingarian, A., Hovsepyan, G., Sargsyan, B., Karapetyan, T., Aslanyan, D., & Kozliner, L. (2024a). Enormous impulsive enhancement of particle fluxes observed on Aragats on May 23, 2023. *Advances in Space Research*. <https://doi.org/10.1016/j.asr.2024.02.041>
- Chilingarian, A., Karapetyan, T., Sargsyan, B., Knapp, J., Walter, M., & Rehm, T. (2024b). Energy spectra of the first TGE observed on Zugspitze by the SEVAN light detector compared with the energetic TGE observed on Aragats. *Astroparticle Physics*, *156*, 02924. <https://doi.org/10.1016/j.astropartphys.2024.102924>
- Chilingarian, A., Khanikyants, Y., Mareev, E., Pokhsranyan, D., Rakov, V. A., & Soghomonyan, S. (2017b). Types of lightning discharges that abruptly terminate enhanced fluxes of energetic radiation and particles observed at ground level. *Journal of Geophysical Research: Atmospheres*, *122*, 7582. <https://doi.org/10.1002/2017JD026744>
- Chilingarian, A., Khanikyants, Y., Rakov, V. A., & Soghomonyan, S. (2020c). Termination of thunderstorm-related bursts of energetic radiation and particles by inverted intracloud and hybrid lightning discharges. *Atmospheric Research*, *233*, 104713. <https://doi.org/10.1016/j.atmosres.2019.104713>
- Chilingarian, A., Kozliner, L., Sargsyan, B., Soghomonyan, S., Chilingaryan, S., Pokhsranyan, D., & Zazyan, M. (2022c). Thunderstorm ground enhancements: Multivariate analysis of 12 years of observations. *Physical Review D*, *106*, 082004. <https://doi.org/10.1103/PhysRevD.106.082004>
- Chilingarian, A., Mirzoyan, R., & Zazyan, M. (2009). Cosmic ray research in Armenia. *Advances in Space Research*, *44*, 1183. <https://doi.org/10.1016/j.asr.2008.11.029>
- Chilingarian, A., & Mkrtchyan, H. (2012). Role of the lower positive charge region (LPCR) in the initiation of the thunderstorm ground enhancements (TGEs). *Physical Review D*, *86*, 072003. <https://doi.org/10.1103/PhysRevD.86.072003>
- Chilingarian, A., Pokhsranyan, D., Zagumenov, F., & Zazyan, M. (2024c). Space-temporal structure of the thunderstorm ground enhancements (TGEs). *Physics Open*, *18*, 100202. <https://doi.org/10.1016/j.physo.2023.100202>
- Chilingaryan, S., Beglarian, A., Kopmann, A., & Voekling, S. (2010). Advanced data extraction infrastructure: A WEB based system for management of time series data. *Journal of Physics: Conference Series*, *219*, 042034. <https://doi.org/10.1088/1742-6596/219/4/042034>
- Chilingarian, A. A., Arakelyan, K., Avagyan, K., et al. (2005). Correlated measurements of secondary cosmic ray fluxes by the Aragats space environmental center monitors. *Nuclear Instruments and Methods in Physics Research Section A: Accelerators, Spectrometers, Detectors and Associated Equipment*, *543*, 483–496. <https://doi.org/10.1016/j.nima.2004.12.021>
- Chilingarian, A. A., Avagyan, K., Babayan, V., et al. (2003). Aragats space-environmental center: Status and SEP forecasting possibilities. *Journal of Physics G: Nuclear and Particle Physics*, *29*, 939–952. <https://doi.org/10.1088/0954-3899/29/5/314>
- Coleman, L. M., Stolzenburg, M., Marshall, T. C., & Stanley, M. (2008). Horizontal lightning propagation, preliminary breakdown, and electric potential in New Mexico thunderstorms. *Journal of Geophysical Research*, *113*, D09208. <https://doi.org/10.1029/2007JD009459>
- Danilova, T. V., Dunaevsky, A. M., Erykin, A. D., et al. (1982). A project of the experiment on the investigation of interactions of hadrons in the energy range 10^3 – 10^5 TeV. In *Proc. Armenian Acad. Sci. Phys. Ser.* (Vol. 17, pp. 129–132). (in Russian).
- Dwyer, J. R. (2003). A fundamental limit on electric fields in air. *Geophysical Research Letters*, *30*, 2055. <https://doi.org/10.1029/2003GL017781>
- Dwyer, J. R. (2007). Relativistic breakdown in planetary atmospheres. *Physics of Plasmas*, *14*, 042901. <https://doi.org/10.1063/1.2709652>
- Dwyer, J. R., Smith, D. M., & Cummer, S. A. (2012). High-energy atmospheric physics: Terrestrial gamma-ray flashes and related phenomena. *Space Science Review*, *173*, 133.
- Fishman, G. J., Bhat, P. N., Mallozzi, R., et al. (1994). Discovery of intense gamma-ray flashes of atmospheric origin. *Science*, *264*, 1313. <https://doi.org/10.1126/science.264.5163.1313>
- Garyaka, A. P., Martirosov, R., Eganov, V., et al. (2002). The cosmic ray energy spectrum around the knee measured with the GAMMA array at Mt. Aragats. *Journal of Physics G: Nuclear and Particle Physics*, *28*, 231–2328.
- Gevorgyan, N., Babayan, V., Chilingaryan, A., & Martirosyan, G. (2005). Test alert service against very large SEP events. *Advances in Space Research*, *36*, 2351–2356. <https://doi.org/10.1016/j.asr.2004.04.016>
- Gurevich, A. V., Milikh, G. M., & Roussel-Dupre, R. A. (1992). Runaway electron mechanism of air breakdown and preconditioning during a thunderstorm. *Physics Letters*, *165A*, 463. [https://doi.org/10.1016/0375-9601\(92\)90348-P](https://doi.org/10.1016/0375-9601(92)90348-P)
- Interferometer. (2024). Retrieved January 1, 2024, from http://crd.yerphi.am/vhf_interferometr/VHF%20INTERFEROMETER%20DATA/
- KCDC. (2024). KASCADE cosmic ray data centre. Retrieved January 1, 2024, from <https://kcdc.ikp.kit.edu/>
- Kelley, N. A., Smith, D. M., Dwyer, J. R., et al. (2015). Relativistic electron avalanches as a thunderstorm discharge competing with

- lightning. *Nature Communications*, 6, 7845. <https://doi.org/10.1038/ncomms8845>
- Lu, G., Cummer, S. A., Blakeslee, R. J., Weiss, S., & Beasley, W. H. (2012). Lightning morphology and impulse charge moment change of high peak current negative strokes. *Journal of Geophysical Research*, 117, D04212. <https://doi.org/10.1029/2011JD016890>
- Nag, A., & Rakov, V. (2009). Some inferences on the role of lower positive charge regions in facilitating different types of lightning. *Geophysical Research Letters*, 36, L05815. <https://doi.org/10.1029/2008GL036783>
- Ostgaard, N., Christian, H. J., Grove, J. E., Sarria, D., Mezentsev, A., Kochkin, P., et al. (2019). Gamma-ray glow observations at 20-km altitude. *Journal of Geophysical Research: Atmospheres*, 124, 7236–7254. <https://doi.org/10.1029/2019JD030312>
- Ostgaard, N., Lang, T. G., Marisaldi, M., et al. (2023). Results from the ALOFT mission: A flight campaign for TGF and gamma-ray glow observations over Central America and the Caribbean in July 2023, AGU, San Francisco 2023, AE22A-03. <https://doi.org/10.5194/egusphere-egu23-3116>
- Torii, T., Sugita, T., Kamogawa, M., et al. (2011). Migrating source of energetic radiation generated by thunderstorm activity. *Geophysical Research Letters*, 38, L24801. <https://doi.org/10.1029/2011GL049731>
- Wada, Y., Matsumoto, T., Enoto, T., et al. (2021). Catalog of gamma-ray glow during four winter seasons in Japan. *Physical Review Research*, 3, 043117. <https://doi.org/10.1103/PhysRevResearch.3.043117>

(Received February 4, 2024, revised March 16, 2024, accepted March 27, 2024)